The numerical challenges in multiphysical modeling of laser welding with arbitrary Lagrangian-Eulerian method

I. Tomashchuk [1] , I. Bendaoud[2,] , J-M. Jouvard [1], P. Sallamand [1]
1. Laboratoire Interdisciplinaire Carnot de Bourgogne – UMR CNRS 6303, Université de Bourgogne – Franche-Comté, Le Creusot, France
2. Laboratoire de Mécanique et Génie Civil, Université de Montpellier, Montpellier, France

Abstract: The interaction of high power laser beam with metallic materials produces a number of interconnected phenomena that represent a serious challenge for numerical modeling, especially for creation of auto-consistent models. Additional difficulty consists in lack of data on materials properties at the temperatures superior to their melting point. The present work summarizes the numerical challenges in creation and validation of free-surface models using ALE moving mesh coupled with heat transfer equation and Navier-Stokes fluid flow.

Keywords: laser welding, metallic alloys, moving mesh, multiphysics.

1. Introduction

ALE method has been successfully used for multiphysical modelling of pulsed[1,2] and continous[2] laser welding, drilling[3], direct laser metal deposition[4] and thermal matter ablation[5]. The displacement of mesh in these models is based on the velocity field calculated with Navier-Stokes equation strongly coupled with heat equation[1-4] or on the property-depending condition[5]. 2D axisymmetric models with µ-metric mesh size allowed an accurate description of the keyhole formation[1,3]. The main limitation of ALE consists in the impossibility to represent the complex modifications of topology, like the formation of bubbles or porosities; however, it provided quite accurate description of free surface movement and good agreement with experimental dimensions of the impact zone. The liquid phase is modelled as an incompressible[2,3] or weakly compressible[1] Newtonian liquid that undergoes laminar flow under the influence of Marangoni convection, natural convection and recoil pressure in the keyhole, produced by the metallic vapor. The recoil pressure that is represented by Clausius-Clapeyron equation or in form of adjusted spatial function is an important factor that determines the depth of the keyhole. To suppress the parasite displacement in the solid part of modelled domain, two approaches exist: to stop the displacement by applying an important frictional dissipation depending on the local fraction of liquid phase (Carman-Kozeny apprroximation[5]) or by introducing temperature-dependent fictive viscosity (for example 100 Pa·s [3] or 1000 Pa·s [2]). The previous models differ in a way to introduce the energy distribution and adsorption coefficient, which is not perfectly known and depends not only on the aggregate state of irradiated matter, but also on local free surface curvature. Another difficulty consists in the lack of data about exact values recoil pressure due to the partial condensation of metallic vapor in the keyhole and about the variation of materials properties in the liquid phase.
The motivation for the present work was determined by the interest to represent both keyhole formation and collapse in a fully auto-consistent 3D model, for further application to multimaterial welding. The modelling in 3D accentuated the convergence problems, mainly because of the limitation of minimal mesh size. Our previous model of dissimilar welding[2] suffered from noticeable lack of weld penetration, compared with experimental results. Moreover, the influence of many numerical (inconsistent stabilization for Navier-Stokes equation, type of ALE smoothing, type of used Navier-Stokes equation) and physical parameters (dynamic viscosity, adsorption coefficient, and condensation coefficient) on the convergence and on the resulting behavior of the impact zone was not fully comprehended. The present work attempts to bring some clarity about the influence of these factors on the simple example of standalone laser pulse applied to the plate of Ti6Al4V alloy.

2. Governing Equations

2.1 Heat transfer

Heat transfer equation was used in time-dependent form:

$$\rho\, c_p{}^{eq}\left(\frac{\partial T}{\partial t}+\vec{U}\cdot\vec{\nabla}T\right)=\vec{\nabla}\cdot\left(\lambda\vec{\nabla}T\right) \quad (1)$$

Laser energy supply is represented by Gauss heat source applied at the top of butt joint. Pulsed laser beam is represented as follows:

$$q_L = \frac{P_L A}{\pi r_0^2} e^{\left(-\frac{x^2+y^2}{r_0^2}\right)} \cdot \left(t < t_{pulse}\right), \qquad (2)$$

where P_L – laser power, $r_{0\,-}$ beam radius and t_{pulse} – pulse duration A - absorption coefficient of laser radiation by each individual material, represented as :

$$A = A_{solid} + (A_{liquid} - A_{solid}) \cdot flc2hs(T-T_m, \Delta T), \qquad (3)$$

where $A_{solid} = 0.4$ and the absorption coefficient in liquid phase increases when the surface temperature nears vaporization temperature:

$$A_{liquid} = A_{surf} + (A_{kh} - A_{surf}) \cdot flc2hs(T-T_v, \Delta T), \qquad (4)$$

where $A_{surf} = 0.25$ and $A_{kh} = 0.8$.

Latent heat of fusion and evaporation are taken in account by means of equivalent enthalpy approach[6]:

$$c_p^{eq} = c_p + D_m . L_m \qquad (5)$$

where C_p is heat capacity as function of temperature, L_f – latent heat of fusion and D_m - Gauss function normalized around melting temperature T_m:

$$D_m = \frac{e^{\frac{-(T-T_m)^2}{\Delta T^2}}}{\sqrt{\pi \Delta T^2}} \qquad (6)$$

where ΔT is smoothing interval of 100 K.

Materials properties of Ti6Al4V are considered as interpolation functions of temperature[7].

2.2 Fluid flow

Liquid metal is assumed as incompressible Newtonian liquid that undergoes laminar flow:

$$\rho\left[\frac{\partial \vec{U}}{\partial t} + \left(\vec{U}\cdot\vec{\nabla}\right)\vec{U}\right] = \vec{\nabla}\cdot\left[-pI + \eta(T)\left(\vec{U}\cdot\vec{\nabla} + \left(\vec{U}\cdot\vec{\nabla}\right)^t\right)\right] + \vec{F} \qquad (7)$$

$$\vec{\nabla}\cdot\vec{U} = 0$$

Metal that has $T<T_m$ is considered as highly viscous fluid, that practically stops all convection movements in solid materials. The transition between solid and liquid material is provided with smoothed Heaviside function:

$$\eta(T) = \eta_{solid} + (\eta_{liquid} - \eta_{solid})\, flc2hs(T-T_m, \Delta T). \qquad (8)$$

Convection movements are generated by following phenomena:

- natural convection described through Boussinesq approximation,
- surface tension force,
- Marangoni convection with $\gamma<0$ introduced in form of weak formulation,
- recoil pressure of vapor filling the keyhole, represented in form of function

$$p_r = \frac{(1+\beta)}{2} \cdot a \cdot e^{-\frac{b}{T}+c} \qquad (9)$$

where the condensation coefficient β = 0.5 and the coefficients *a,b, c* for Ti6Al4V are given by Kaidalov[8].

2.3 Free surface

Present study uses ALE moving mesh approach for representing the movements of free surface. The advantage of this method consists in possibility to neglect the vapor phase and thus lighten the calculation. The weak point consists in limitations of free surface movement: the formation of droplets or bubbles in the melted zone is forbidden by the impossibility to break or unite individual meshes. Movement of free surface is determined by the velocity field in the melted zone.

2.4. Numerical implementation

Present model involves *Heat Transfer in Fluids*, *Laminar flow* and *Moving Mesh* modules that are strongly coupled and solved with time-depended solver. Multiphysics coupling is ensured by the interrelation between heat transfer and Navier-Stokes equations: velocity field in heat equation is provided by resolution of Navier-Stokes equation, when temperature field defines thermophysical properties of the liquid involved in convection process. Consistent (streamline and crosswind) stabilization and inconsistent stabilization (isotropic diffusion) were applied to Navier-Stokes equation. Consistent stabilization was also applied to the heat transfer equation. Moving Mesh solves surface deformation in function of locally calculated velocity field.

Only one plate (3mm x 2mm x 2mm) is modelled for symmetry reasons. Tetrahedral mesh of 250 µm maximal size is applied over calculation domain. The top surface of is meshed with 50 µm.

The models were solved on work station with Intel 2.20 (2 processors, 44 cores) and 256 Gb RAM.

3. Experimental study

Welding experiments were carried out with pulsed Nd:YAG laser of 3 kW maximal power and focused beam diameter (∅) of 560 µm.

Laser beam was focused on the surface of butt joint between 2 mm thick Ti6Al4V plates. Standalone pulses with duration of 4 and 6 ms and power 1.5 kW were realized. Three standalone pulses per condition were made.

The penetration of pulses at the joint line was measured by breaking the weld and observing Ti6Al4V side of joint plane with optical microscope.

4. Discussion

4.1 Comparison between the different methods of mesh smoothing

The main challenge in use of ALE for modelling of keyhole welding consists in rapid surface deformation, which is associated with quite severe elongation of meshes. In the first place, the performances of different smoothing methods were compared (Figure 1, Table 1). The Laplace smoothing (Figure 1.a) led to the rapid divergence after interaction time of only 1.5 ms, associated with quite high distortion of the elements. The Yeoh smoothing (Figure 1.b) allowed to extend the calculation up to only 3.2 ms, followed by divergence, in spite of low estimated distortion of the elements. Parasite ripple-like surface deformation was observed in the solid around the melted zone. The Winslow smoothing (Figure 1.c) allowed to reach the end of laser pulse (6 ms), however the aspect of free surface is very rough and the width of the keyhole is highly overestimated. Finally, the use of hyperelastic smoothing (Figure 1.d) allowed the most accurate keyhole representation, associated with quite low distortion of the elements. This formulation allows attaining the maximal deformation of free surface, and thus is the most appropriate for this kind of simulation, in accordance with conclusion of Bruyere et al.[1] However, the important deformation of the meshes situated at the center of laser pulse leads to the loss of mesh quality at the bottom of the keyhole. These preliminary calculations were performed with inconsistent Navier-Stokes stabilization δ_{id} = 1 and mean viscosity of solid of 100 Pa·s.

Table 1: The comparison of ALE smoothing methods

Smoothing	Convergence	Element distortion	Δz_{KH}[a] (µm)
Laplace	No	12.84	120
Yeoh	No	1.10	301
Winslow	Yes	7.20	477
Hyperelastic	Yes	3.2	532

[a] maximal keyhole depth

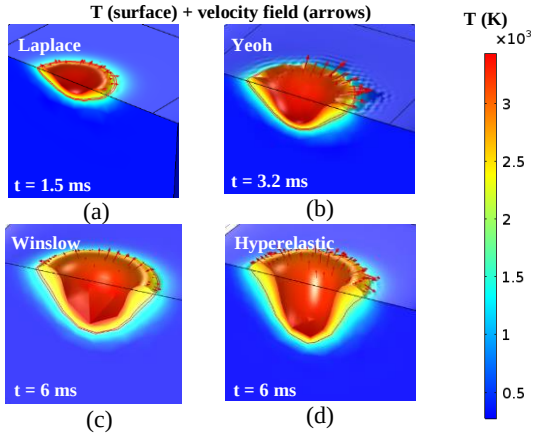

Figure 1. The comparison of ALE smoothing methods applied to the model of pulsed welding of Ti6Al4V (t_{pulse} = 6 ms, ∅=560 µm, P_L= 1.5 kW).

4.2 The influence of numerical stabilization of Navier-Stokes equation

In absence of inconsistent Navier-Stokes stabilization, the model is likely to diverge at the moments corresponding to sudden rise of velocity field, as, for example, during the collapse of the keyhole at the end of the pulse. In general way, the increase of δ_{id} value promotes the smoothing of velocity field and better convergence, but the excessive values can alter the observed phenomenology. The values of δ_{id} of 1 (default) and 0.5 were compared (Table 2). The calculations were performed with mean viscosity of solid of 100 Pa·s. It can be concluded that melt depth is not at all sensitive to the reduction of δ_{id} value, and makes small effect on melted zone width (ΔW = -124 µm), maximal melt temperature (ΔT = -16K) and velocity (ΔU = +0.2 m/s). The default value of δ_{id}=1 was conserved for the rest of the calculations.

Table 2: The effect of inconsistent stabilization

δ_{id}	MZ (µm)		T_{max} (K)	U_{max} (m/s)
	Depth	Width		
1	611	1454	3380	1.6
0.5	611	1330	3364	1.8

4.3 The effect of viscosity formulations

Another important numerical problem is the parasite velocity field in the solid material. It was observed that the mean viscosity of solid of 100 Pa·s produces unphysical relaxation of already solidified matter in the ring formed around the zone of the impact (Figure 2). Cutting off the velocity field in the solid area using temperature or viscosity-based condition in ALE module is not enough, because, as it was found, the fictive viscosity of the solid makes important influence on interaction phenomenology. An insufficient value of solid viscosity makes an important influence on temperature evolution of the melt and fluid dynamics. The evolution of the impact zone under standalone laser pulse can be divided in four major stages: the initiation of the keyhole (Figure 3.a), the progression of the keyhole (Figure 3.b), the keyhole collapse (Figure 3.c) and the solidification resulting in final surface profile with the ring around the impact zone and slight depression in its center (Figure 3.d).
The main characteristics of the process and the evolution of maximal temperature, velocity field and keyhole depth for solid viscosity values of 100 and 200 Pa·s are illustrated in Table 3 and Figure 4 respectively. The increase of solid viscosity has important impact on calculation time. Moreover, higher values of solid viscosity (≥300 Pa·s) leads to the convergence problems.

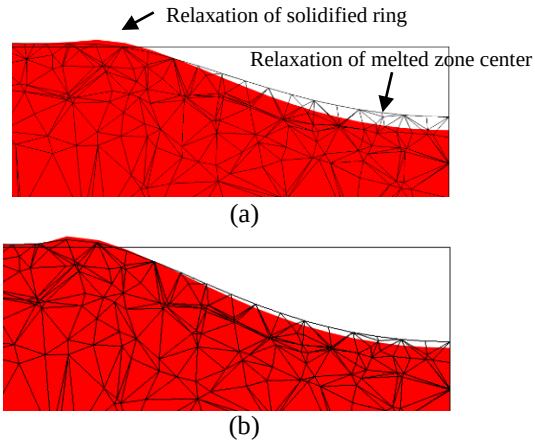

Figure 2. Unphysical relaxation of solidified weld between t = 14 ms (end of solidification) and t = 20 ms (wireframe) for solid viscosity of (a)100 Pa·s and (b) 200 Pa·s.

The main difference between the cases with η_{solid} of 100 Pa·s and of 200 Pa·s consists in the intensity of keyhole initiation process. The application of high viscosity of the solid impedes the "parasite" lateral evacuation of the heat from impact zone, because the residual convection in solid material is efficiently reduced. This results in sudden progression of the keyhole depth starting from 1.5 ms with maximal temperature of 4480 K at the center of the impact and the velocity of the liquid reaching 7 m/s. The solid viscosity of 100 Pa·s does not produce such peak of temperature and velocity: during all keyhole life they remain at the plateau of ~3380 K and ~1.6 m/s. The sudden progression of the keyhole for the case of 200 Pa·s results in 80 µm more profound keyhole.

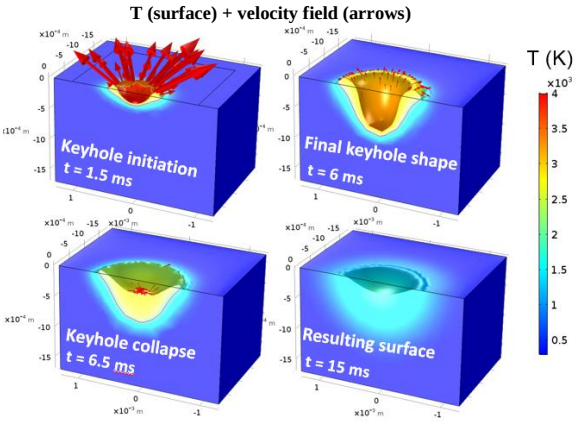

Figure 3. Nd:YAG laser pulse on Ti-6Al-4V plate (6 ms, 1.5 kW, Ø = 560 µm). η_{solid} = 200 Pa·s.

Two calculations produce the similar evolution of the maximal temperature on the stage of keyhole progression and collapse, however, higher solid viscosity results in little higher speed of collapsing liquid (~2.45 m/s compared to 1.55 m/s).

Table 3: The effect of mean viscosity of the solid

η_{solid} (Pa·s)	MZ (µm)		T_{max} (K)	U_{max} (m/s)	Calculation time (h)
	Depth	Width			
100	611	1454	3380	1.6	4h57
200	828	1324	4480	7.5	72h24
Hf [a]	698	1450	4870	10.0	144h52

[a] Heaviside function , equation 10

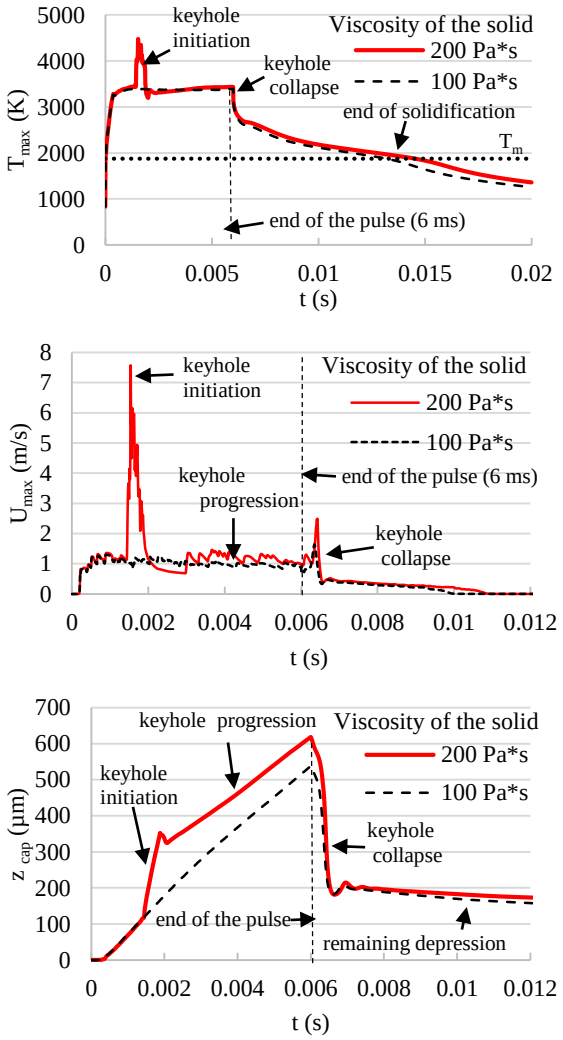

Figure 4. The influence of solid viscosity on the evolution of maximal temperature, melt velocity and keyhole depth for standalone Nd:YAG laser pulse on Ti-6Al-4V plate (1,5 kW, Ø = 560 µm).

Higher solid viscosity also produces more tardive completion of the solidification of the melt: 15.5 ms compared to 14 ms for 100 Pa·s. It also modifies the proportion of the melt, making it more profound and less large (Table 3). In spite of quite similar keyhole depth (~530 µm), the case with 200 Pa·s results in 217 µm deeper melt, when the thickness of the melted zone is reduced at 130 µm. The comparison with the

average experimental dimensions of the melted zone speaks in advantage of higher solid viscosity (Table 4). For both η_{solid} values, the depth of the melt is underestimated, when the width is correct, however higher solid viscosity results in deeper melt. The experimental weld was produced on two distinct plates, when numerically only the condition of symmetry is applied on the joint line, which can partially explain such high difference between calculated and experimental values. The simplified representation of absorption in the keyhole and the lack of information about recombination coefficient β influencing the recoil pressure (equation 9), along with the difficulties of accurate numerical resolution of keyhole bottom, are likely to be responsible for underestimation of melt depth. The increase of solid viscosity has an immediate effect on calculation time, multiplied roughly by 16 (Table 3). The attempt to apply the gradual decrease of fictive viscosity with temperature (Heaviside function, equation 10) can be used to stabilize the numerical solution and produces the behavior of the melt similar to the use of high (200 Pa·s) solid viscosity, however, very important calculation time makes this approach unattractive.

$$\eta_{solid} = \eta_{cold} + (\eta_{hot} - \eta_{cold})\ flc2hs(T-900, \Delta T) \qquad (10)$$

Table 4: The comparison with experimental weld dimensions

Experimental dimensions of the melted zone (µm)				
Test 1	1055	1286	1269	1553
Test 2	1059	1349	1259	1426
Test 3	1008	1332	1222	1379
Average	1041	1322	1250	1453
η_{solid} (Pa·s)	Relative error (%)			
	after 4 ms		after 6 ms	
	Depth	Width	Width	Depth
100	57.0	10.2	8.0	51.0
200	47.0	9.6	9.0	34.0
Hf[a]	48.6	3.2	0.3	44.2

[a] Heaviside function

The effect of the viscosity in the liquid phase also was analyzed: the temperature-dependent formulation (equation 11 considered by default in all calculations) was compared with constant value if $T>T_m$ (Table 5). As the viscosity of liquid decreases with temperature, in the first case the digging of the melted zone is facilitated and consequently the higher depth of the melt is obtained. However, no important effect was noticed on the maximal melt velocity or temperature, as well as on weld width. The behavior of the liquid zone is quite similar (Figure 5).

$$\eta_l = \begin{cases} -4\cdot10^{-6}\cdot T + 0.0118 & \text{if} \quad T_m < T \le 2500K \\ 1.5\cdot10^{-3} & \text{if} \quad T > 2500K \end{cases} \qquad (11)$$

Table 5: The effect of viscosity of the liquid

η_{liquid} (Pa·s)	Melted zone dimensions (µm)		T_{max} (K)	U_{max} (m/s)	Calculation time (h)
	Depth	Width			
f(T) [a]	828	1324	4480	7.5	72h24
$4\cdot10^{-3}$	725	1358	4400	7.5	82h23

[a] equation 11

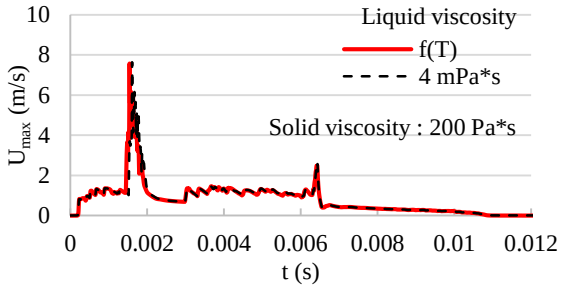

Figure 5. The influence of liquid viscosity on the evolution of maximal melt velocity for standalone Nd:YAG laser pulse on Ti-6Al-4V plate (P_L= 1.5 kW, Ø = 560 µm).

4.4 The influence of keyhole absorption coefficient

The absorption coefficient in the keyhole makes a strong influence on maximal surface temperature, and thus on the resulting recoil pressure (equation 9). The parametric study for A_{kh} values from 0.6 to 0.9 was carried out. In these calculations, dynamic viscosity was considered as function of temperature (equation 11) for the liquid and 200 Pa·s for the solid.

It was found that the shift from 0.7 to 0.8 produces an important shift in keyhole depth, associated with rise of maximal temperature and velocity field (Table 6). For $A_{kh} \le 0.7$, the first peak in velocity field associated with rapid digging of the keyhole is absent, and the velocities associated with the collapse of the keyhole are also lower (Figure 6). To reach the realistic values of penetration, it is needed to use high adsorption coefficients 0.9-1, but it this cases the convergence was not reached for the moment.

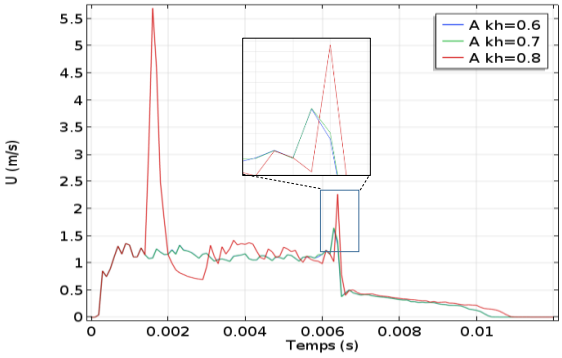

Figure 6. The influence of keyhole absorption coefficient on the evolution of melt velocity for standalone Nd:YAG laser pulse on Ti-6Al-4V plate (1.5 kW, Ø = 560 µm).

Table 6: The effect of keyhole absorption coefficient

A_{kh}	T max (K)	U max (m/s)	MZ (μm)	
			Depth	Width
0.6	3445	2.28	587	1308
0.7	3460	2.28	587	1308
0.8	4480	5.5	828	1324
0.9	No convergence			

4.5 The influence of condensation coefficient

The condensation coefficient represents the variation of surface pressure in function of evaporation conditions (equation 9): from β = 0.17 for strong evaporation to β = 1 for full thermodynamic equilibrium[9]. Strong evaporation diminishes the surface pressure (Figure 7), which can influence the keyhole formation. By default, the value of β = 0.5 is admitted in our calculations. Lower values of β resulted in convergence problems. The parametric study was performed for β = 0.5 – 1.

It was found that for β > 0.5 the intense initiation of keyhole formation is absent, which traduces by lower weld penetration, temperature and melt velocity (Table 7). Melted zone width is not very sensible to the variation of β. For β = 0.6 – 1, quite similar depths of the melted zone, maximal temperatures and maximal velocities of the melt (associated with keyhole collapse) are observed.

Table 7: The effect of condensation coefficient

β	MZ (μm)		T_{max} (K)	U_{max} (m/s)
	Depth	Width		
0	No convergence			
0.4	No convergence			
0.5	828	1324	4480	7.5
0.6	589	1308	3440	2.34
0.7	594	1312	3420	2.18
0.8	597	1308	3400	2.04
0.9	600	1314	3390	2.04
1	600	1318	3380	2.04

It looks like the increase of β (and so the recoil pressure) slows down the digging of the keyhole, which seems unphysical. The observation of relative pressures at weld cross-section at the end of the pulse (Figure 7.b) shows the zones of maximal pressure at the bottom of the keyhole, which seems physical, but also around the ring of ejected matter, where the displacement of the meshes is blocked by the absence of velocity field. This second maximum is a numerical artifact with no physical significance, as well as the zones of low pressure situated at the solid material beneath. This local increase of pressure may impede the ejection of liquid from the keyhole, which explains why low melt depth for β > 0.5.

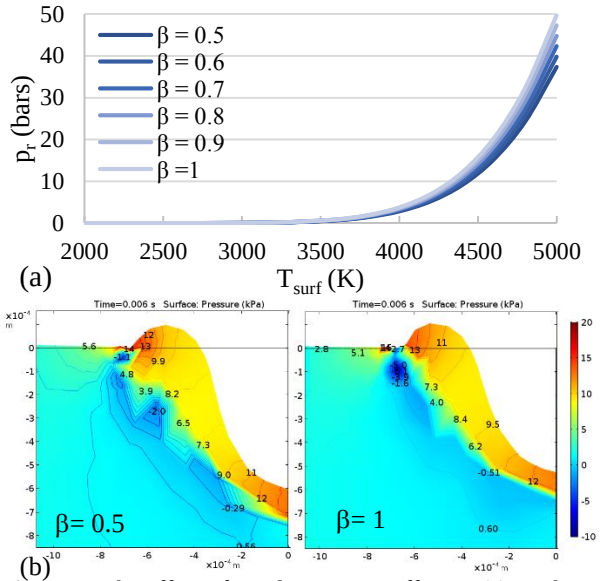

Figure 7. The effect of condensation coefficient (a) on the rise of recoil pressure with temperature and (b) on the relative pressure field at the end of the pulse (t= 6 ms).

4.6 Comparison of incompressible and weakly compressible Navier-Stokes equations

Axisymmetric ALE-based model of keyhole digging proposed by Bruyere et al.[1] showed slight loss of mass of the domain. The same problem was noticed in the present 3D model. In the calculations performed with incompressible Navier-Stokes formulation, the noticeable loss of mass produces during the creation of the keyhole (Figure 8). It is proportional to the maximal deformation of the domain and took place for both considered values of solid viscosity. After the collapse of the keyhole, the relaxation of strained meshes allows to "recover" some missing mass, but not completely, which results in the situation when the depression in the center of solidified melt is not fully compensated by the height of solidified ring around the melt. Weakly compressible Navier-Stokes equation offers good mass conservation (Figure 8), comparable with result of Bruyere et al.[1], however, the convergence of the models is more difficult due to higher temperature and velocity gradients and more rapid deterioration of element quality. For instance, only the association of compressible Navier-Stokes formulation with Heaviside function for solid viscosity (equation 10) allowed to reach the convergence along with good mass conservation.

The different values of solid viscosity produce different effect in incompressible and weakly compressible Navier-Stokes equations (Table 8). For solid viscosity of 100 Pa·s, the reduction of penetration depth is negligible and the maximal residual depression in the impact center increased by only 20

μm. For higher solid viscosity, the melt becomes ~ 130 μm less profound, and there is no impact on residual depression.

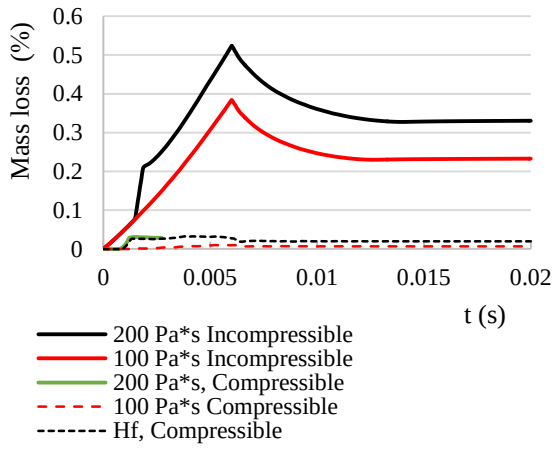

Figure 8. Mass conservation compared for incompressible and compressible Navier-Stokes formulations.

Table 8: The effect of Navier-Stokes formulation

Navier-Stokes	η_{solid} (Pa·s)	Controlled dimensions (μm)	
		Meted zone depth	Impact center depression
Incompressible	100	611	125
	200	828	150
Compressible	100	596	144
	Hf [a]	698	150

[a] Heaviside function

Conclusions

1. Hyperelastic deformation seems the most appropriate for the modelling keyhole evolution.
2. The velocity field not sensible to the inconsistent stabilization coefficient for Navier-Stokes at the range 0.5-1.
3. Low viscosity of the solid phase not only produces parasite relaxation of solidified domain, but can completely alter the phenomenology of laser/metal interaction. Thus at least 200 Pa·s value is recommended. The solution is much less sensible to the formulation of viscosity in the liquid phase. However, temperature-dependent viscosity promotes the digging of the keyhole.
4. Keyhole adsorption coefficient is the key parameter that controls surface temperature and melt depth. The shift from 70% to 80% adsorption produces the qualitative change in the dynamics of keyhole progression, with much more intense digging in the beginning of the pulse. Higher value would create even more profound weld, and thus reach experimentally observed penetration, but it is associated with too severe mesh deformation producing the convergence problems. This problem can be treated with different remesing approaches that increase the time of calculation to the high degree.
5. The condensation coefficient of 0.5 seems the most appropriate. Higher values impede the digging of the keyhole because unphysical accumulation of pressure around the ejection ring, and lower values produce convergence problems.
6. The shift from incompressible or weakly compressible Navier-Stokes formulation does not alter the observed phenomenology and allows better mass conservation. However, it is likely to be more sensible to the convergence problems.

References

1. V.Bruyere, C. Touvrey, P. Namy, Comparison between Phase Field and ALE methods to model the keyhole digging during spot laser welding, *COMSOL Conference Rotterdam (2013).*
2. I. Tomashchuk, I. Bendaoud, P. Sallamand, E. Cicala, S. Lafaye, M. Almuneau. Multiphysical modelling of keyhole formation during dissimilar laser welding, *COMSOL Conference Munich (2016).*
3. S. Sharma, Y. Pachaury, S.N. Akhtar, J. Ramkumar, A study of hydrodynamics of melt expulsion in pulsed Nd:YAG laser drilling of titanium. *COMSOL Conference Pune (2015).*
4. S. Morville, M. Carin, M Muller, M. Gharbi, P. Peyre, D. Carron, P. Le, 2D axial-symmetric model for fluid flow and heat transfer in the melting and resolidification of a vertical cylinder, *COMSOL Conference Paris (2010).*
5. W. Frei, Modeling Thermal Ablation for Material Removal, *COMSOL blog*, March 30, 2016.
6. C. Bonacina, G. Comini, A. Fassano, M Primicerio, Numerical solutions of phase change problems, *Int. J. Heat Mass Transfer*, **16**, 1825-1832 (1973).
7. S. Morville, Modélisation multiphysique du procédé de fabrication directe par projection laser, *phD thesis, Université de Bretagne-Sud*, France (2012).
8. A.A. Kaidalov, Electron beam welding and annexed technologies (in Russian), Kyiv, Technologia (2004).
9. R. Fabbro. Quelques processus physiques présents en régime de soudage par keyhole. Ecole thématique CNRS Laser'ApE, 2-5 October 2017, Nouan-le-Fuzelier, France.

Acknowledgements

This work was carried out as a part of joint laboratory project LabCom FLAMme between Laboratoire Interdisciplinaire Carnot de Bourgogne, University of Bourgogne-Franche Comté and SME Laser Rhone-Alpes. This project is funded by French National Agency of Research.